JBC RESEARCH ARTICLE

Structural basis for c-di-AMP–dependent regulation of the bacterial stringent response by receptor protein DarB

Received for publication, June 1, 2022, and in revised form, June 9, 2022 Published, Papers in Press, June 15, 2022,
https://doi.org/10.1016/j.jbc.2022.102144

Jana L. Heidemann[1,‡], Piotr Neumann[1,‡], Larissa Krüger[2], Dennis Wicke[2], Liza Vinhoven[1], Andreas Linden[3,4], Achim Dickmanns[1], Jörg Stülke[2], Henning Urlaub[3,4], and Ralf Ficner[1,*]

From the [1]Department of Molecular Structural Biology, and [2]Department of General Microbiology, Institute for Microbiology & Genetics, GZMB, Georg-August-University Göttingen, Göttingen, Germany; [3]Bioanalytical Mass Spectrometry, Max Planck Institute for Multidisciplinary Sciences, Göttingen, Germany; [4]Bioanalytics, Institute for Clinical Chemistry, University Medical Center Göttingen, Göttingen, Germany

Edited by Wolfgang Peti

The bacterial second messenger c-di-AMP controls essential cellular processes, including potassium and osmolyte homeostasis. This makes synthesizing enzymes and components involved in c-di-AMP signal transduction intriguing as potential targets for drug development. The c-di-AMP receptor protein DarB of *Bacillus subtilis* binds the Rel protein and triggers the Rel-dependent stringent response to stress conditions; however, the structural basis for this trigger is unclear. Here, we report crystal structures of DarB in the ligand-free state and of DarB complexed with c-di-AMP, 3′3′-cGAMP, and AMP. We show that DarB forms a homodimer with a parallel, head-to-head assembly of the monomers. We also confirm the DarB dimer binds two cyclic dinucleotide molecules or two AMP molecules; only one adenine of bound c-di-AMP is specifically recognized by DarB, while the second protrudes out of the donut-shaped protein. This enables DarB to bind also 3′3′-cGAMP, as only the adenine fits in the active site. In absence of c-di-AMP, DarB binds to Rel and stimulates (p)ppGpp synthesis, whereas the presence of c-di-AMP abolishes this interaction. Furthermore, the DarB crystal structures reveal no conformational changes upon c-di-AMP binding, leading us to conclude the regulatory function of DarB on Rel must be controlled directly by the bound c-di-AMP. We thus derived a structural model of the DarB–Rel complex *via in silico* docking, which was validated with mass spectrometric analysis of the chemically crosslinked DarB–Rel complex and mutagenesis studies. We suggest, based on the predicted complex structure, a mechanism of stringent response regulation by c-di-AMP.

The cystathionine β-synthase (CBS) domain is a small protein motif consisting of ca. 60 aa. It was first identified in several archeal proteins and the name-giving human CBS (1). Up to now, it was found in all kingdoms of life in a plethora of proteins that exhibit a large variety of functions (2, 3). Some of these proteins consist only of CBS domains, while in many other proteins the CBS domains are fused to other domains. Many CBS domains regulate the activity of enzymes and membrane transporters dependent on ligands bound to the CBS domains (4). Most CBS domains bind AMP, or ATP, or other adenosine derivatives like NAD or SAM. Another recently identified adenosine derivative bound by CBS domains is the bis-(3′-5′)-cyclic dimeric AMP (c-di-AMP) (5, 6). c-di-AMP is a bacterial second messenger involved in many cellular processes that binds to several different proteins as well as to an RNA riboswitch (7–10). Furthermore it is the only second messenger in bacteria known to be both essential for viability and toxic upon accumulation, since it regulates the activity of proteins required for potassium and osmolyte homeostasis (11), and binding of c-di-AMP to potassium ion transporters blocks potassium import (12–14), respectively. c-di-AMP does not only bind to CBS domains but also to other receptors, for example, PII-like signal transduction proteins (15), the KUP family potassium transporters KupA/B and KimA (16–18), USP-like domains (19), and RCK_C domains present in some potassium transporters (20). Binding of c-di-AMP to the CBS domains of the OpuCA subunit of the carnitine transporter OpuC leads to an inhibition of carnitine uptake (5, 6). The Mg^{2+} transporter MgtE is another CBS domain protein, which binds c-di-AMP and is also involved in osmolyte transport (18). All these functions render c-di-AMP an essential molecule in several signaling pathways. This secondary messenger is synthesized by diadenylate cyclases, which are absent in mammalian cells (21). Loss of the c-di-AMP synthesizing enzymes is lethal to the bacterial cell (7). Since its discovery in 2008, numerous studies have reported the presence of c-di-AMP in a wide range of different bacterial species, of which several are well-known human pathogens, for example, *Listeria monocytogenes*, *Mycobacterium tuberculosis*, *Borrelia turicatea*, *Enterococcus faecium*, *Staphylococcus aureus*, and *Streptococcus pneumoniae* (22–24). With the exception of *M. tuberculosis*, these bacteria use the diadenylate cyclase CdaA as the sole enzyme responsible for c-di-AMP synthesis. Interestingly, the latter three pathogens belong to the 12 bacterial families that pose the greatest threat to human health according to the World Health Organization (https://www.who.int/news/item/27-02-2017-who-publishes-list-of-bacteria-for-which-new-antibiotics-are-urgently-needed).

‡ These authors contributed equally to this work.
* For correspondence: Ralf Ficner, rficner@uni-goettingen.de.

Accordingly, the essential diadenylate cyclase CdaA has become a promising target for the development of new antibiotics. Since the essentiality of c-di-AMP depends on its signaling function, it is reasonable that the c-di-AMP–binding proteins are also interesting candidates as drug targets.

All CBS domains share the same topology (β_1–α_1–β_2–β_3–α_2), but they often display only low sequence conservation within protein families or even within one protein. The first two of the three β-strands are in a parallel orientation, while the third one is in an antiparallel orientation relative to the first two. The β-strands β2 and β3 are flanked by two α-helices (α1 and α2). Usually, CBS domains occur as pairs or quads and each pair is forming a tandem repeat domain, also denoted as Bateman module (2, 3). This fold is often stabilized by the region positioned N-terminally to the conserved CBS motif containing a third α-helix (α0), which clamps the two CBS domains in a tandem repeat. There are three different types of homodimers formed by CBS domains, classified as parallel (head-to-head assembly), antiparallel (head-to-tail assembly), and V-shaped (3). The structural and/or functional benefits that favor a significantly greater abundance of parallel CBS assemblies in nature (95%) as compared to the antiparallel modules are not well understood (3). The parallel and antiparallel dimers exhibit a disk-like shape and contain four CBS domains related by an internal D_2 pseudosymmetry, the so-called CBS module. The tandem repeat of two CBS domains contains two canonical adenosine-binding sites; hence, a dimeric protein with four CBS domains could bind up to four adenosines.

Recently, the CBS domain protein DarB/CbpB (previously denoted as YkuL) was identified as c-di-AMP–binding protein in *Bacillus subtilis* and *L. monocytogenes*, respectively (18, 25). DarB consists of 147 aa forming a CBS tandem repeat and comprises two CBS domains but no other domains.

DarB binds to the GTP pyrophosphokinase Rel and thereby stimulates (p)ppGpp synthesis in a ribosome-independent manner. This interaction as well as DarB-stimulated (p)ppGpp synthesis is suppressed in the presence of c-di-AMP (26). (p)ppGpp formation is part of the stringent response of bacterial cells under amino acid starvation or other stress conditions (27, 28). In addition, apo-DarB also binds to the pyruvate carboxylase to stimulate the replenishment of the citric acid cycle (29).

Here, we demonstrate that DarB specifically binds c-di-AMP with a dissociation constant in the nanomolar range and AMP with much lower affinity. DarB also binds 3′3′-cGAMP *in vitro*; however, as cGAMP does not exist in *B. subtilis*, this interaction might have no physiological relevance but might reveal interesting possibilities for drug development. In order to understand the specificity and affinity for different ligands, we determined four crystal structures of DarB, in its apo from and its ligand bound form either with c-di-AMP, 3′3′-cGAMP, or AMP, respectively. The four CBS domains of the homodimeric DarB bind two molecules of c-di-AMP; however, only one adenine of each c-di-AMP is specifically recognized by DarB, while the second adenine protrudes out of the donut-like shaped homodimer. This protruding adenine most likely prevents the DarB–Rel interaction, since no conformational changes occur in DarB upon c-di-AMP binding, which could cause the loss of protein–protein interaction. Furthermore, we suggest a 3D model of the Rel–DarB complex, which is based on computational docking experiments validated by mass-spectrometric analysis of crosslinked complexes and by binding studies with mutated DarB.

Results

Nucleotide binding and specificity of DarB

The CBS domain containing protein DarB from *B. subtilis* was recently identified as a c-di-AMP–binding protein (18). Since CBS domains are known to bind a plethora of adenine-containing nucleotides, isothermal calorimetry (ITC) measurements with different mononucleotides and dinucleotides were performed in order to determine the nucleotide affinity and specificity of DarB (Fig. 1). The results confirmed the tight binding of c-di-AMP with a K_D in the nanomolar range (27.0 nM ± 1.98 nM). No binding was detected for 2′3′-cGAMP, c-di-GMP, ATP, SAM, NAD^+, and CoA (Fig. S1). Interestingly, 3′3′-cGAMP binds to DarB with a K_D in the low micromolar range (1.17 μM ± 0.97 nM) and also an even weaker interaction with AMP was observed (K_D of 91.1 μM ± 14.2 μM) (all ligands with 1:1 M stoichiometry). The direct comparison of the binding constants of 3′3′-cGAMP and c-di-AMP reveals that DarB binds the cyclic homodinucleotide with an approximately 40-fold higher affinity than the cyclic heterodinucleotide. However, since 3′3′-cGAMP is absent in *B. subtilis*, its binding to DarB has most likely no physiological relevance but raises the question of how this could be achieved. Hence, we decided to structurally characterize AMP and 3′3′-cGAMP DarB complexes and investigate if these weak interactions resemble c-di-AMP binding.

Crystal structure of DarB

DarB crystallized in the orthorhombic space group $P2_12_12_1$ with two DarB molecules occupying the asymmetric unit. The crystal structure of the ligand-free DarB (DarB-apo) was determined at 1.84 Å resolution (Table 1) and superposes well with the deposited but unpublished structure of DarB/YkuL (Protein Data Bank [PDB] ID: 1YAV) and CbpB (PDB ID: 6XNU), as indicated by the r.m.s.d. of 0.53 Å and 1.23 Å between all Cα atoms, respectively (30). The previously deposited structure 1YAV represents a different crystal form of DarB without any nucleotide bound.

The DarB monomer occurs as tandem repeat of two CBS domains (CBS1 and CBS2), both possessing the canonical βαββα fold and an N-terminal region that contains a short α-helix and in case of CBS1 also a short β-strand (Fig. 2*A*). The N-terminal region preceding the CBS1 spans over the two CBS domains and clamps them together, as the N terminus of the polypeptide chain is positioned close to the C terminus of the CBS2. The N-terminal short β-strand (β0) of CBS1 packs against β-strand β6 of CBS2 and extends the β-sheet of CBS2 as the fourth strand, thereby stabilizing the arrangement of the two CBS domains. The core of the protein is formed by the β-sheets of CBS1 and CBS2. These two β-sheets are oriented

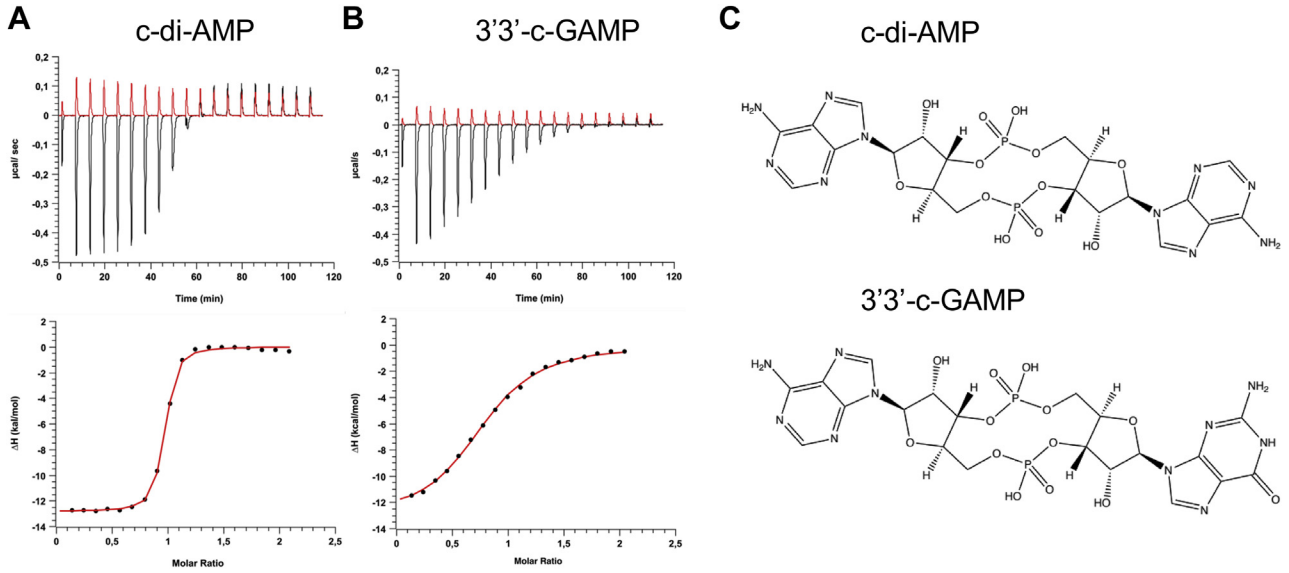

Figure 1. Nucleotide binding measured by means of ITC. *A*, the nucleotide-based second messenger c-di-AMP specifically binds to DarB with a K_D of 27.0 nM ± 1.98 nM. *B*, the hetero dinucleotide 3′3′ cGAMP binds to DarB with an approximately 40-fold lower affinity in comparison to c-di-AMP. Both ligands bind with 1:1 M stoichiometry to DarB. *C*, chemical structure of the ligand c-di-AMP and 3′3′-c-GAMP. c-di-AMP, cyclic dimeric AMP; ITC, isothermal calorimetry.

parallel to each other and are flanked on each side by the α-helices. Similarly, to the N-terminal region, the linker connecting CBS1 and CBS2 also contains an α-helix (α0-1) followed by the canonical CBS fold of CBS2 (β4-α4-β5-β6-α5).

The two molecules occupying the asymmetric unit form a donut-shaped homodimer related by a twofold noncrystallographic symmetry. The dimer interface buries 1402.8 Å^2 of the accessible surface area (17.5%) and is stabilized by seven hydrogen bonds formed between residues comprising α-helices 1 and 1′ as well as α-helices 4 and 4'. According to the CBS protein classification, DarB forms a dimer in a parallel head-to-head assembly (Fig. 2*B*). The donut-shaped DarB homodimer has a predominantly negatively charged outer surface, while the surface of its central pore is positively charged (Fig. 2*C*).

Structure of DarB–c-di-AMP complex

DarB was also crystallized in the presence of a few adenine-containing nucleotides that were identified by our ITC measurements (see previous text). Firstly, DarB was cocrystallized

Table 1
Crystallographic data collection and refinement statistics

PDB code	DarB-apo 6YJ8	DarB-c-di-AMP 6YJA	DarB-AMP 6YJ7	DarB-cGAMP 6YJ9
Crystallographic data				
Beamline	Petra III-P13, EMBL, Hamburg	Petra III-P13, EMBL, Hamburg	Petra III-P14, EMBL, Hamburg	Petra III-P14, EMBL, Hamburg
Wavelength (Å)	0.97625	0.97625	0.97625	0.97625
Resolution range (Å)[a]	41.24–1.84 (1.88–1.84)	40.91–1.70 (1.76–1.70)	41.94–1.64 (1.71–1.64)	35.68–1.50 (1.52–1.50)
Unique reflections	24,397	32,669	37,896	50,229
Redundancy	5.1 (5.3)	7.0 (7.3)	13.25 (13.52)	12.95 (13.34)
Completeness (%)	99.1 (99.7)	99.8 (99.8)	99.8 (99.8)	99.9 (100)
Space group	$P2_12_12_1$	$P2_12_12_1$	$P2_12_12_1$	$P2_12_12_1$
a (Å)	38.67	42.15	41.31	41.49
b (Å)	67.76	65.41	69.26	69.92
c (Å)	103.96	104.85	105.42	105.78
R_{merge} (%)	5.8 (64.0)	5.2 (92.0)	2.9 (68.0)	3.9 (63.2)
I/ σ (I)	16.81 (2.51)	24.45 (2.41)	40.44 (4.12)	31.06 (4.2)
$CC_{1/2}$	99.8 (87.3)	99.9 (88.6)	100 (97.4)	100 (94.2)
Refinement statistics				
R_{work}/R_{free}	0.2023/0.2509	0.1828/0.2105	0.1885/0.2204	0.1532/0.1907
No. of atoms	2418	2586	2488	2780
Average B factor (Å^2)	36.53	30.90	44.34	31.42
RMSD				
Bonds Å	0.005	0.007	0.011	0.009
Angles (degree)	0.775	1.062	1.138	1.145
Ramachandran plot				
Favored (%)	98.15	99.26	98.51	98.18
Allowed (%)	1.85	0.74	1.49	1.82
Outliers (%)	0.00	0.00	0.00	0.00

[a] Values for the data in highest resolution shell are shown in parentheses.

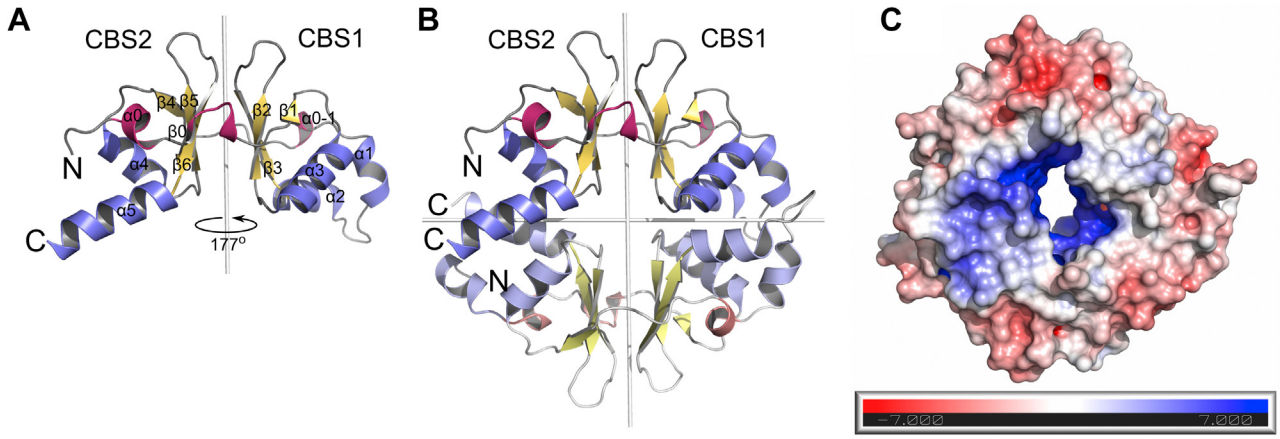

Figure 2. Crystal structure of DarB. *A*, the structure of DarB monomer is depicted in cartoon representation (helices: *blue*, b-strands: *yellow*, linker region: *red*, loop region: *gray*). Each DarB monomer occurs as a tandem repeat which is composed of two CBS domains (CBS1 and CBS2), possessing canonical βαββα fold. *B*, DarB forms a donut-shaped dimer in a parallel head-to-head assembly placing the N and C termini close to each other. *C*, the electrostatic surface potential of DarB exhibits a mainly negatively charged outer surface with a prominent positively charged patch connected to the highly positively charged central pore. Surface is ramp colored from $-7k_BT/e$ (*red*) to $+7k_BT/e$ (*blue*).

with c-di-AMP. The obtained crystals belong to the same space group as the ligand-free DarB crystals but differ slightly in unit cell dimensions. The structure of the c-di-AMP–DarB complex was determined at 1.70 Å resolution (Table 1) and superposes well with the apo structure (r.m.s.d. of 0.52 for all 274 Cα atoms), as well as with the published structure of the c-diAMP–CbpB complex (PDB ID: 6XNV) from *L. monocytogenes*, as indicated by the r.m.s.d. of 1.21 Å for 121 common Cα atoms (1.34 Å for 241 Cα atoms) (25). It should be noted that the structure 6XNV represents a different crystal form; hence, the observed identical homodimeric oligomerization state of DarB and CbpB is not a result of crystal packing. Both structures share 52.7% of sequence identity and the same binding mode of c-di-AMP in a well-conserved binding site (Fig. S10) (25).

The two DarB molecules in the asymmetric unit form the donut-shaped dimer like the apo DarB. The difference electron density map clearly revealed the presence of two c-di-AMP molecules bound inside the donut-shaped DarB dimer (Fig. S2). The c-di-AMP molecules are bound in a compact conformation with the adenine bases in an almost coplanar orientation, which has been denoted as U-type and was previously also shown for CbpB (Fig. S10) (9).

The nucleotide-binding site is formed by the loop region connecting α1 and β2 as well as β-strand 2 of CBS1, α-helix 4 and β-strands 5 and 6 of CBS2, and α-helix 4 of the CBS2 of the other monomer (B) (Fig. 3*A*). Residues Lys23, Ala25, Tyr45, Thr46, Ala47, and Arg132 of monomer A and Arg131′ of monomer B are involved in c-di-AMP binding (Fig. 3, *B* and *C*). The N6 of the adenine-1 (Ade1) forms a hydrogen bond to the main chain carbonyl O atom of Lys23 and N1 to the backbone N atom of Ala25. Furthermore, Tyr45 positioned in the loop α1-β2 stacks with the adenine in an almost coplanar orientation. Surprisingly, the second adenine (Ade2) does not show any direct interactions with the protein. It protrudes from the protein ring and is surrounded by several water molecules, of which two are mediating contacts between adenine-2 and the protein. The 2′-OH of the ribose attached to Ade1 is hydrogen bonded to the carbonyl O atom of Ala47. The 2′-OH and the 3′-O of the second ribose (adenosine-2) form hydrogen bonds to side chain of Arg131′ of the other monomer. The phosphate of adenosine-1 forms hydrogen

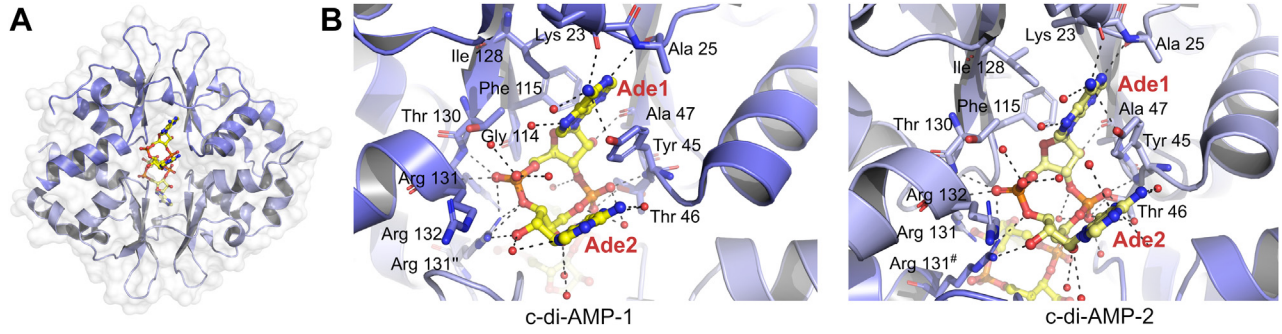

Figure 3. Crystal structure of DarB with two nucleotide-binding sites. *A*, cartoon representation of the donut-shaped homodimeric DarB with two bound c-di-AMPs. Monomer A is colored in *dark blue*; monomer B is colored in *light blue*. The two c-di-AMP molecules are depicted in *ball and stick mode* (carbon: *yellow*, phosphate: *orange*, nitrogen: *blue*, oxygen: *red*). *B*, a detailed view of the nucleotide-binding site in monomer *A* and *B*, showing amino acids involved in the c-di-AMP binding. Only one adenine base is coordinated by amino acids, while the other protrudes out of the protein core and coordinated through water molecules. The *dashed lines* indicate polar interactions between the ligand and surrounding atoms up to 3.2 Å. c-di-AMP, cyclic dimeric AMP.

bonds with the main chain N of Arg132, while the phosphate of adenosine-2 forms two hydrogen bonds with the side chain OH and the main chain amide of Thr46.

The structure of the DarB–c-di-AMP complex superposes well with the ligand-free DarB structure. Hence, binding of c-di-AMP does not induce any major conformational changes in DarB, although some minor structural changes occur in the central pore of the protein dimer. In the ligand-free state, the central pore of the dimer is constricted in comparison to the c-di-AMP–bound state. This structural change is due to a movement of the loop connecting α1 and β2, which leads to a repositioning of Thr46. Upon c-di-AMP binding, this loop becomes less flexible as Thr46 forms a hydrogen bond with the phosphate of the ligand and is therefore fixed in its position. Another difference between apo and ligand-bound state concerns the side chain of Tyr45, which is disordered in the ligand-free state. When c-di-AMP is bound Tyr45 is caught in one conformation by the π–π stacking interaction with the adenine base.

Structure of DarB–AMP complex

Since the ITC experiments also showed a weak binding of AMP to DarB, crystallization trials of DarB in presence of AMP were performed. The obtained crystals diffracted to a resolution of 1.64 Å and belonged to the same space group as observed for the DarB–c-di-AMP and apo-DarB structures. The difference electron density maps (2mFo-DFc and mFo-DFc) demonstrate two AMP molecules bound in the position corresponding to the two adenosine-1 moieties in the c-di-AMP complex structure (Fig. S3). Hence, the protein–AMP contacts are the same as for the corresponding Ade-1 of c-di-AMP (Fig. 4). The comparison of the two nucleotide-binding sites in the DarB–AMP complex unveiled that in one of the monomers the side chain of Arg132 binds the phosphate of AMP, while in the other monomer Arg132 is rotated outward of the binding pocket and forms a salt bridge with the Asp9 of a symmetry-related protein molecule leading to the loss of the contact with the AMP phosphate. The observed flexibility of Arg132 side chain could explain the higher K_D of AMP in comparison to 3′3′-cGAMP and c-di-AMP and indicate a huge impact of the cyclic phosphate moiety on binding affinity.

Structure of DarB–3′3′-cGAMP complex

As the ITC experiments revealed that the heterodinucleotide 3′3′-cGAMP is also bound by DarB, but not the related 2′3′-cGAMP, this complex was crystallized as well. The DarB crystals obtained in presence of 3′3′-cGAMP belong also to the space group $P2_12_12_1$ and contain two protein monomers in the asymmetric unit as described for DarB in complex with c-di-AMP. The crystal structure was determined at 1.50 Å resolution, and the difference electron density unveiled the presence of two 3′3′-cGAMP molecules bound in a similar manner as c-di-AMP (Fig. S4). The binding of the adenine moiety in 3′3′-cGAMP is identical to that of Ade1 of c-di-AMP, while the guanine base is protruding out of the protein ring like the Ade2 in the c-di-AMP complex. Surprisingly, the difference electron density maps indicated the presence of two additional 3′3′-cGAMP molecules adjacent to one of the two canonically bound 3′3′-cGAMP, here denoted as cGAMP-2 (Figs. S4 and S5). The guanine of the third 3′3′-cGAMP (cGAMP-3) molecule interacts with the protruding guanine of cGAMP-2 by π–π stacking between the bases. The symmetric arrangement of cGAMP-2 and cGAMP-3 results in a similar intermolecular hydrogen-bonding pattern: both guanine NH2 groups interact with phosphate moieties and N7 of the neighboring cGAMP molecule. The fourth 3′3′-cGAMP molecule (cGAMP-4) forms π–π stacking interaction of its adenine with the guanine of cGAMP-3; hence, the guanine of cGAMP-3 is sandwiched between the guanine of cGAMP-2 and the adenine of cGAMP-4 (Fig. 5). cGAMP-4 interacts with the protein by several hydrogen bonds formed between the phosphates and the side chains of Lys23, Lys136, Arg132, and between the guanine and the main chain carbonyl O of Phe17 and Met18. Notably, the weaker electron density for cGAMP-3 and cGAMP-4 corresponds to a lower occupancy of 58% and 59%, respectively, meaning that the third and fourth 3′3′-cGAMP is bound to only ca. 60% of the DarB protein molecules in the crystal. These additional 3′3′-cGAMP molecules are involved in water-mediated interactions to neighboring molecules in the crystal lattice. This suggests that crystal packing

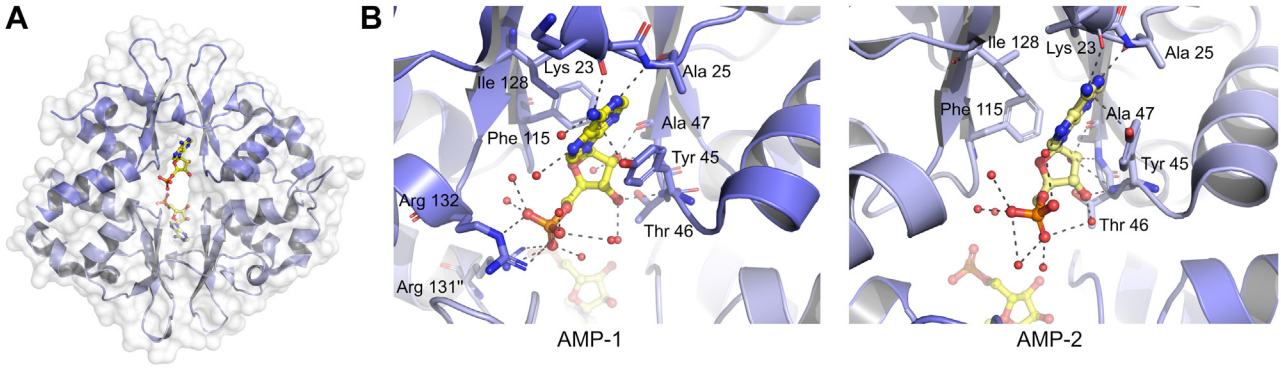

Figure 4. Crystal structure of DarB in complex with AMP. *A*, cartoon representation of the DarB with two bound AMPs. Monomer A is colored in *dark blue*; monomer B is colored in *light blue*. The two AMP molecules are depicted as *ball* and *stick* (carbon: *yellow*, phosphate: *orange*, nitrogen: *blue*, oxygen: *red*). *B*, a detailed view of the nucleotide binding in molecule *A* and *B*. The *dashed lines* indicate polar interactions between the ligand and surrounding atoms up to 3.2 Å.

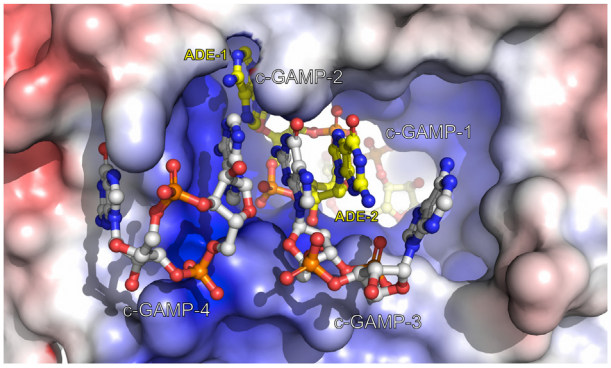

Figure 5. Crystal structure of DarB in complex with 3′3′-cGAMP. In this structure two additional 3′3′-cGAMP molecules (cGAMP-3 and cGAMP-4) are bound to DarB adjacent to one of the two canonically bound 3′3′-cGAMP (cGAMP-1). The additional 3′3′-cGAMP molecules are bound along the positive patch on the protein surface and interact *via* π–π stacking with the protruding guanine of the 3′3′-cGAMP located in the c-di-AMP binding site. The nucleotides are depicted as *ball* and *stick* (phosphate: *orange*, nitrogen: *blue*, oxygen: *red*, canonical 3′3′-cGAMP: carbon: *yellow*; noncanonical 3′3′-cGAMP: carbon: *gray*). c-di-AMP, cyclic dimeric AMP.

could be responsible for the binding of the additional 3′3′-cGAMP molecules. The binding of these not canonically bound 3′3′-cGAMP molecules could not be confirmed by ITC measurements (Fig. 1) supporting the 1:1 M stoichiometry.

Interaction between Rel^{NTD} and DarB

Recently the GTP pyrophosphokinase Rel was identified as interaction partner of DarB/CbpB (25, 26). Rel consists of an N-terminal part (NTD) that harbors the the (p)ppGpp synthase (SYN) and hydrolyzing (HYD) domains and a C-terminal part containing the regulatory domains. Previous studies have already shown that DarB binds to the NTD of Rel (26).

To elucidate how Rel and DarB interact with each other and which surface areas of both proteins are involved, *in silico* blind docking experiments have been performed with ClusPro (https://cluspro.bu.edu/login.php; Vajda Lab and ABC Group; Boston University and Stony Brook University) and ROSETTA (https://www.rosettacommons.org/software) using known 3D structures of homodimeric DarB and monomeric Rel (PDB ID: 6YJ8 (DarB), 6YXA (Rel) (31),). The best scoring *in silico* models have been validated by spatial restraints derived from mass spectrometry (MS) crosslinking experiments of purified Rel–DarB complex (Fig. S8). Additionally, results of DarB–Rel binding studies with mutated DarB allowed further validation of the complex models. The design of DarB mutants was performed in PyMOL (www.pymol.org/) by visual inspection of the best scoring complex models with the focus of finding crucial residues located on the protein–protein interface and concomitantly not being involved in c-di-AMP binding. Leucine 38 (L38) of DarB has been identified as a residue facing, with its side chain, a hydrophobic patch formed by L385 and L389 (Rel). Mutating L38 to a bulkier residue, like phenylalanine, should cause intermolecular clashes preventing Rel binding (Fig. S9). An even bulkier residue, like tryptophan, would cause intramolecular clashes within DarB, hence is not adequate. A large polar residue, like arginine or lysine, would most likely find an interaction partner and due to its flexibility prevent formation of clashes with Rel. The second residue subjected to mutagenesis studies, N68 of DarB, faces a polar cleft formed by main chain of M382 and side chains of E383 and S384 in Rel. When mutated to tyrosine, three out of the four most likely side chain conformers (rotamers) would cause intramolecular clashes with neighboring residues (DarB) leaving only one conformation, which could be adopted in an unbound state. This side-chain conformation, however, causes severe intermolecular clashes with Rel according to our complex model and hence should prevent complex formation (Fig. S9). Docking-based designed single point mutations of L38F as well as N68Y of DarB almost completely abolished binding of DarB to Rel NTD in ITC experiments and thus confirmed the validity of the predicted model (Fig. S6 and Table S2). These mutated DarB proteins were still able to bind c-di-AMP, indicating that the mutations did not corrupt the protein fold (Fig. S7). The location of DarB residues A25 and R132, which were previously shown to be involved in Rel binding (26), is also in agreement with the docking model, although these two residues are forming the c-di-AMP–binding site and thus might also influence the dinucleotide binding. (Fig. 6).

In order to further optimize the position of DarB molecule placed on the top of the Rel NTD, spatial restraints derived from MS crosslinking experiment have been used for high resolution docking experiments, which yielded the final model of the Rel–DarB complex (Fig. 6). In the proposed model of Rel–DarB complex, the DarB molecule interacts mostly with the outer surface of α-helices 7 and 16, which connect the SYN and HYD subdomains with each other, and in addition with a short linker region, which connects α16 directly to the TGS domain. The TGS domain of Rel was suggested to be involved in the regulation of (p)ppGpp synthesis and hydrolysis through its association with α14 of the SYN domain (31). Most importantly, the proposed model explains how c-di-AMP suppresses the Rel–DarB complex (Fig. 6, *B* and *C*), as c-di-AMP bound to DarB prevents complex formation due to steric clashes between the protruding adenine ring (Ade-2) and residue E367 of Rel.

Discussion

The bacterial second messenger c-di-AMP regulates a broad range of cellular processes such as cell wall homeostasis, stress responses, potassium uptake and export, DNA damage responses, and central metabolism. To fulfill these functions, c-di-AMP has to bind to rather different proteins and as well to an RNA riboswitch (10).

In order to understand how c-di-AMP regulates the function of target proteins, their 3D structures in the c-di-AMP–bound state and the ligand-free state have to be analyzed. The crystal structures of the c-di-AMP receptor DarA/PstA revealed a PII signal transduction protein fold. The trimeric DarA binds three c-di-AMP molecules and undergoes large conformational changes of the T and the B loops upon c-di-AMP binding, which is thought to mediate the signaling

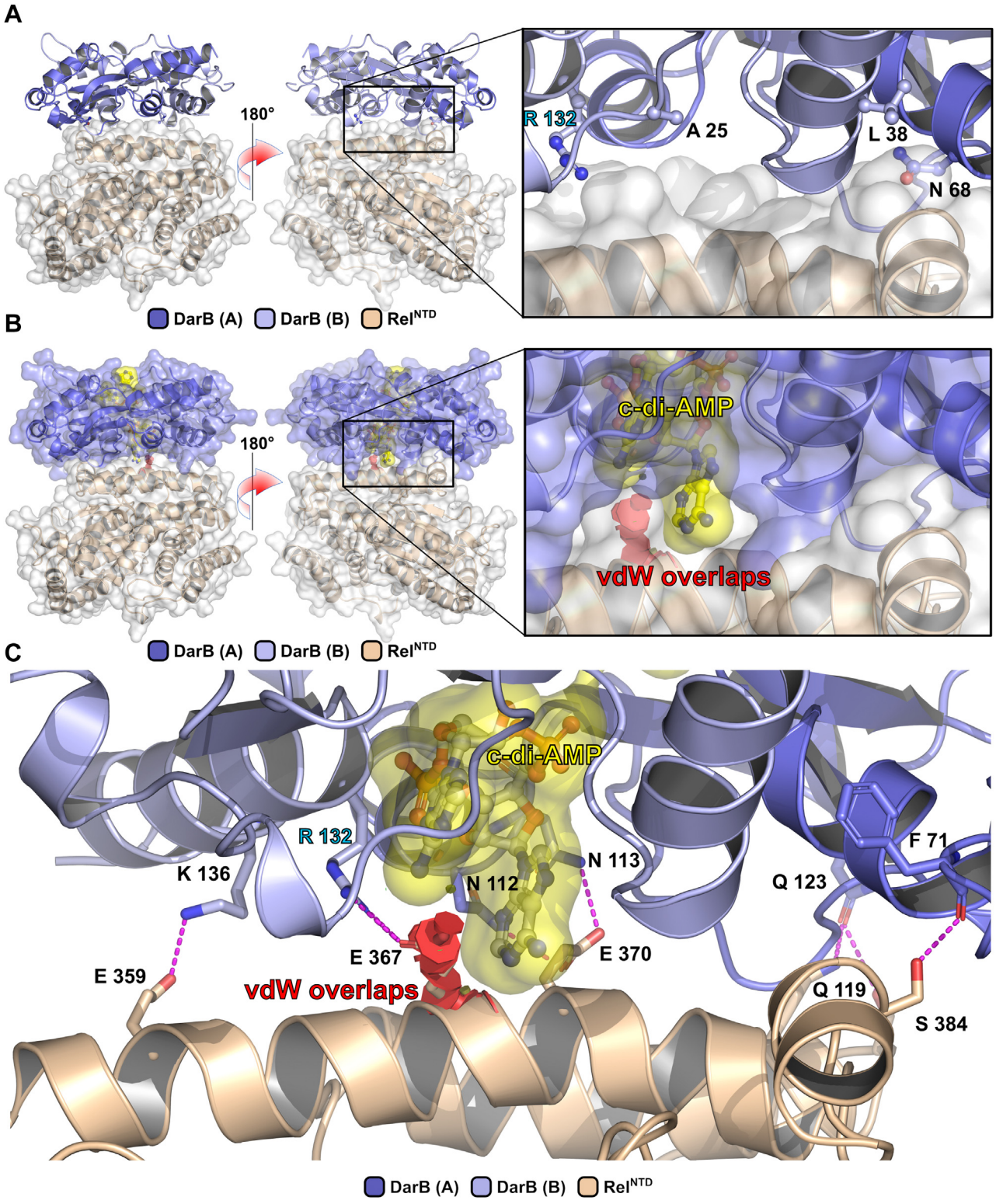

Figure 6. DarB–Rel^{NTD} docking-based molecular model. *A*, an overview of DarB–Rel complex. On the left, a close-up view of the protein–protein interface with mutated residues (depicted in *sticks*) subjected to site-directed mutation experiments confirming the validity of the complex model. The c-di-AMP molecule (*balls* and *sticks*) is shown for clarity and easier comparison with (*B*) and (*C*), which are represented in the same orientation of the complex. R132 and A25 form the binding site, L38 and N68 are located distal to it. *B*, c-di-AMP (*ball* and *stick* model surrounded by *yellow* surface) prevents complex formation due to steric clashes (Van der Waals overlaps depicted as *red octagonal disks*) between protruding adenine ring (Ade-2) and residue E367 of Rel. *C*, interface of DarB–Rel complex with steric clashes caused by c-di-AMP. Polar interactions (maximal distance 3.2 Å) are marked as *magenta dashed lines*. Important for complex formation is the interaction of R132 of DarB with Rel E367. The later would clash with Ade-2 ring when cdi-AMP is bound to DarB. c-di-AMP, cyclic dimeric AMP.

function (15). Another c-di-AMP–binding protein of known 3D structure is the pyruvate carboxylase, which is allosterically inhibited by c-di-AMP due to induced large conformational changes (20, 32). The structures of the RCK_C domains of KtrA (14) and CpaA (30) could not reveal how c-di-AMP affects the ion transporter activity, as this might require the structure of the entire transporter and not just of a protein domain (14). Similarly, the crystal structure of the CBS domain of the carnitine transporter subunit OpuCA could not unveil the mechanism of allosteric inhibition caused by c-di-AMP (5). However, for both the potassium and the carnitine transporter, an induced conformational change mechanism has been suggested that affects transporter activity. Hence, c-di-AMP binding induces conformational changes in all these proteins, which most likely trigger the regulatory function.

Most strikingly, in the case of DarB the mechanism appears to be very different, as the protein structure does not change significantly upon c-di-AMP binding. This indicates that the suppression of the DarB–Rel interaction must be caused directly by the bound c-di-AMP. The proposed structure of the Rel–DarB complex shows that the protruding adenine of the bound c-di-AMP prevents Rel–DarB association, implying a competition, as Rel binds to the same region of the DarB surface as c-di-AMP.

Under stress conditions, like amino acid starvation, the GTP pyrophosphokinase Rel binds to the ribosome, which leads to an activation of the alarmone (p)ppGpp synthesizing activity and simultaneously to the inhibition of its hydrolyzing function. It was suggested that in the absence of stress signals, Rel dissociates from the ribosome and transitions into an autoinhibited state. This autoinhibited state was proposed to be facilitated by the association of the C-terminal subdomain TGS with the N-terminal subdomain SYN (31). Structural data of the *B. subtilis* protein Rel unveiled a direct interaction between β-strand 7 and 8 of the TGS domain and α-helix 14 positioned in the SYN domain. This probably leads to a remodeling of its active site and therefore a repressed synthesis of the alarmone synthase. Furthermore, it was assumed that this remodeling transduces an allosteric signal resulting in a stimulation of the HYD domain (31). Recently, two independent studies showed that Rel-catalyzed (p)ppGpp synthesis can be stimulated in *B. subtilis* and *L. monocytogenes* independent of the ribosome through the binding of DarB (25, 26). Based on our model, we assume that DarB prevents the interaction of the TGS domain with the SYN domain trough α helix 14 and Rel stays in an (SYN/ON HYD/OFF) elongated form as it is described while binding to the ribosome. Furthermore, *via in silico* docking and mutation experiments, we could identify two DarB residues that are crucial for the binding between Rel^{NTD} and DarB (L38F and N68Y). Interestingly, Peterson *et al.* (25) identified two mutations in the *L. monocytogenes* DarB counterpart CbpB at the same position as described here for DarB. These suppressor mutants were isolated in a DarB overexpression experiment with DarB carrying an amino exchange to L38H and D68V. Based on our results, one can assume that these mutations in CbpB also result in a reduced binding affinity of CbpB to Rel in *L. monocytogenes*.

The affinity of DarB for c-di-AMP (K_D of 43 nM) is comparable to that of DarA (15) and RCK_C (14) but about 100-fold higher than the affinity of the OpuCA CBS domain (5). The binding of c-di-AMP by the CBS domains of OpuCA and DarB differs largely. The most important difference between OpuCA and DarB concerns the stoichiometry, as the four CBS domains of OpuCA harbor just one c-di-AMP molecule, while in DarB the four CBS domains bind two c-di-AMP molecules (Fig. S6). This might be a consequence of the different dimer assemblies, which is parallel in DarB and antiparallel in OpuCA (Fig. S6). In OpuCA the c-di-AMP adopts an extended (O-type) conformation, and both adenines are bound, while in DarB the c-di-AMP has a compact (U-type) conformation with the two adenines in an almost coplanar orientation and just one adenine of each c-di-AMP is bound by the protein. Despite these differences, the mode of recognition of the AMP moiety is similar. In OpuCA, both adenines of c-di-AMP are bound by stacking interaction with a tyrosine side chain and hydrogen bonds of the N1 and N6 with main chain amide and carbonyl of a valine residue and the N7 with OH group of a threonine residue. The phosphate group is bound by an arginine side chain.

The structure of DarB with 3′3′-c-GAMP revealed the binding of two additional cGAMP molecules adjacent to one of the canonically bound cGAMP molecules. The stacking arrangement of these three interacting cGAMP molecules and their binding to the DarB surface is reminiscent of a single-stranded nucleic acid. Notably, nucleic acid binding had been reported for the CBS domain of inosine 5′monophosphate dehydrogenase, which binds ssDNA and ssRNA (33), and the CBS domain protein MJ0729, which binds dsDNA (34). However, structural insights into nucleic acid binding by CBS domains have remained elusive, and there is currently no experimental evidence for nucleic acid binding by DarB.

Under conditions of potassium starvation, the essential cellular process of translation is severely compromised. Thus, apo-DarB that prevails under these conditions can bind to Rel and trigger the formation of the alarmone (p)ppGpp. As a consequence, many cellular activities are reprogrammed including a switch off of translation. The results presented here suggest why apo-DarB and not c-di-AMP–bound DarB can interact with Rel and thus provides a molecular understanding of this important regulatory process.

The network of c-di-AMP dependent regulatory processes, that are crucial for survival and growth of bacterial cells, has been intensively investigated within the last 10 years. This has paved the way for starting the development of antibiotics targeting c-di-AMP synthesizing enzymes, in particular CdaA. In addition, the downstream effectors of c.di-AMP, including DarB are likely to turn out as new potential drug targets. The binding of nonphysiological ligands such as 3′3′-c-GAMP suggests a route to identify substances that may interfere with DarB signal transduction.

Experimental procedures

Mutagenesis

Transformation of *Escherichia coli* and plasmid DNA extraction were performed using standard procedures (35). All

commercially available plasmids, restriction enzymes, T4 DNA ligase, and DNA polymerases were used as recommended by the manufacturers. Chromosomal DNA of *B. subtilis* was isolated as described (36). *B. subtilis* was transformed with plasmid and genomic DNA according to the two-step protocol (36).

All DarB mutants were generated by a standard protocol of the combined chain reaction using an additional 5′-phosphorylated primer to introduce the desired mutation (37). The resulting plasmids were pGP2972 (*darB*), pGP3481 (*darB*-L38F), and pGP3477 (*darB*-N68Y).

Protein expression and purification

E. coli Rosetta (DE3) was transformed with the previously described plasmids pGP2972 encoding 6x-His-SUMO-DarB (26) or pGP3429 encoding 6xHis-Rel^{NTD} (26). Expression of the recombinant proteins was induced by the addition of IPTG (final concentration, 1 mM) to exponentially growing cultures (A_{600} of 0.8) of *E. coli* carrying the relevant plasmid. Cells were lysed by three passes at 18,000 p.s.i. through an HTU DIGI-F press (G. Heinemann). After lysis (DarB: 50 mM Tris–HCl pH 7.5, 150 mM NaCl; Rel: 50 mM Tris–HCl pH 8.3, 200 mM NaCl), the crude extract was centrifuged at 100,000*g* for 60 min and then passed over a Ni^{2+}-nitrilotriacetic acid column (IBA). The protein was eluted with an imidazole gradient. After elution, the fractions were tested for the desired protein using 15% SDS-PAGE. The relevant fractions were combined, and for DarB, the SUMO tag was removed with the SUMO protease while overnight dialysis. The cleaved SUMO moiety and the protease were removed using a Ni^{2+}-nitrilotriacetic acid column. For crosslinking experiments, Rel^{NTD} and DarB were mixed, incubated for 10 min at room temperature, and loaded onto a Superdex S200 (Cytiva) size-exclusion chromatography column (20 mM Hepes pH 7.5, 150 mM NaCl). Protein concentration was determined according to the method of Bradford (38) using the Bio-Rad dye binding assay and bovine serum albumin as standard (Bio-Rad).

ITC

All ITC experiments were performed on a VP-ITC microcalorimeter (MicroCal Inc). Prior to the ITC measurements the buffer of the protein solution was exchanged using the "Zaba" spin desalting columns (Thermo Scientific) to 50 mM Tris–HCl pH 7.5, 200 mM NaCl. The nucleotides were individually dissolved in the same buffer (c-di-AMP, c-di-GMP, 3′3′c-GMP-AMP, 2′3′c-GMP-AMP, AMP, and ATP). Measurements were carried out with 10 μM DarB in the sample cell and 100 μM nucleotide in the titration syringe. For the identification of differences in affinity toward Rel^{NTD} comparing DarB WT and mutants, all proteins were dialyzed against the same buffer (50 mM Tris–HCl pH 8.3, 200 mM NaCl). The experiments were carried out with 10 μM Rel^{NTD} in the sample cell and 100 μM DarB mutant in the titration syringe. All experiments were carried out at 20 °C and a stirring speed of 307 rpm. All parameters for the titration series are given in Table S1. The data analysis was carried out using the MicroCal PEQ-ITC Analysis, Malvern Panalytical software. The protein and ligand concentration were determined by using either the Bradford assay (38) or a Nanodrop spectrophotometer (NANODROP 2000 Spectrometer, Thermo Scientific).

Crystallization and cryoprotection

The sitting-drop vapor diffusion method was applied for all crystallizations. Initial crystallization trials with droplets consisting of 1 μl protein solution and 1 μl of reservoir solution were performed at 20 °C using the protein at a concentration of 4.0 mg/ml. For crystallizing the DarB-apo, the droplet size was increased to 2 μl using the 1:1 protein-to-reservoir ratio. Rectangular-shaped crystals grew overnight in 0.2 M calcium acetate, 0.1 M Mes pH 6.5, 15% w/v PEG 8000. For crystallization of DarB–c-di-AMP complex, the protein was supplemented with a sixfold excess of ligand (Jena Bioscience). The best diffracting crystals grew after approximately 24 h in 0.2 M calcium chloride dehydrate, 0.05 M Hepes sodium pH 7.5, 28% v/v PEG 400 and 0.002 M spermine (Hampton Research) in a 1:1 ratio (0.25 μl: 0.25 μl of protein/reservoir).

Both crystal types were soaked in a sucrose-saturated reservoir solution for cryoprotection and flash cooled before data collection.

DarB was also crystallized in presence AMP or 3′3′-cGAMP. A protein concentration of 4.5 mg/ml DarB supplemented with either an 8.5-fold excess AMP or a 6.0-fold excess of 3′3′-cGAMP in a 1:1 protein-to-reservoir ratio. In case of AMP best diffracting crystals were obtained after 1 month, while DarB-3′3′-cGAMP containing crystals were already obtained after 24 h in 0.1 M Tris–HCl pH 8.5, 32% w/v PEG 4000 and 5% v/v glycerol, respectively. No additive was added to the reservoir solution for cryoprotection.

X-ray data collection and processing

The diffraction images were recorded at PETRA III EMBL beamlines P13 (DarB_apo and DarB_c-di-AMP) and P14 (DarB_AMP and DarB_3′3′-cGAMP) and processed with the XDS package (39, 40). The data collection and processing statistics are summarized in Table 1. For all crystals an orthorhombic lattice with similar unit cell parameters was determined. The crystals of apo DarB and in complex with AMP exhibit unit cell parameters of a = 38.670 Å, b = 67.760 Å, c = 103.960 Å, and a = 41.310 Å, b = 69.260 Å, c = 105.420 Å, respectively. The crystals in complex with c-di-AMP and 3′3′-cGAMP exhibit cell constants of a = 42.150 Å, b = 65.410 Å, c = 104.850 Å and a = 41.840 Å, b = 65.130 Å, c = 104.210 Å, respectively. The cell content analysis of all four structures indicated the presence of two monomers occupying the asymmetric unit (apo: V_m = 2.07 Å^3/Da, corresponding solvent content 42.61%, c-di-AMP: V_m = 2.15 Å^3/Da, corresponding solvent content of 42.81%, 3′3′cGAMP: V_m = 2.15 Å^3/Da, corresponding solvent content 42.73%, and AMP: V_m = 2.27 Å^3/Da, corresponding solvent content 45.89%).

Structure determination and refinement

The initial phases of DarB_c-di-AMP were obtained by molecular replacement with PHASER (41) using the DarB structure of *B. subtilis* (PDB ID: 1YAV) as a search model. All other structures (DarB_apo, DarB_3′3′-cGAMP and DarB_AMP) are isomorphous to the DarB_c-di-AMP crystal structure. Therefore, rigid body refinement followed by manual modeling in Coot (42) utilizing 2mFo-DFc and mFo-DFc electron density maps was performed. Reciprocal space refinement has been conducted with Refmac5 (43) and PHENIX (https://phenix-online.org/) (44). In order to monitor the progress of refinement using the R_{free}, a random set of 5% reflections was excluded from the refinement. The structure of DarB_apo was determined at a resolution of 1.84 Å and to R_{work} of 20.23% and R_{free} of 25.09%. The final structure of DarB in complex with c-di-AMP was determined at a resolution of 1.70 Å to R_{work} of 18.28% and R_{free} of 21.05%. Finally, the structures of DarB in complex with AMP and 3′3′-cGAMP were determined at 1.64 Å (R_{work} of 18.85% and R_{free} of 22.04%) and 1.50 Å (R_{work} of 15.32% and R_{free} of 19.07%) resolution, respectively. Atomic models have been verified against omit maps as calculated with PHENIX suite. The presence of bound ligands has been confirmed by calculation of omit maps using phenix.polder program (45). Figures have been generated using an open source version of PyMOL.

Rel^{NTD}–DarB crosslinking and MS

The purified DarB–Rel^{NTD} complex was crosslinked with 2 mM BS3 in combination with 10 mM sulfo-NHS (Thermo Fisher Scientific) for 2 h on ice. The crosslinking reaction was quenched with 50 mM Tris–HCl.

Crosslinked proteins were reduced with 5 mM tris(2-carboxyethyl)phosphine and subsequently alkylated with 20 mM chloroacetamide. Proteins were digested with the endoproteinase trypsin in an enzyme-to-protein ratio of 1:50 in the presence of 1 M urea at 37 °C overnight. The reaction was terminated with 0.5% TFA (v/v), and peptides were desalted on MicroSpin Columns (Harvard Apparatus) following manufacturer's instructions. Vacuum-dried peptides were resuspended in 50 µl 30% acetonitrile/0.1% TFA. Crosslinked peptides were enriched by peptide size-exclusion chromatography (46) (Superdex Peptide 3.2/300 column, GE Healthcare). Fractions of 50 µl were collected. Early eluting fractions that contain crosslinked peptides were subjected to LC-MS/MS analysis.

Crosslinked peptides were measured in technical duplicates on a QExactive HF Mass Spectrometer coupled to a Dionex UltiMate 3000 UHPLC system (both Thermo Fisher Scientific) equipped with an in house-packed C18 column (ReproSil-Pur 120 C18-AQ, 1.9 µm pore size, 75 µm inner diameter, 30 cm length, Dr Maisch GmbH). Peptides were separated applying the following gradient: mobile phase A consisted of 0.1% formic acid (v/v), mobile phase B of 80% acetonitrile/0.08% formic acid (v/v). The gradient started at 5% B, increasing to 10%, 15%, or 20% B within 3 min (according to fraction), followed by a continuous increase to 48% B within 45 min, then keeping B constant at 90% for 8 min. After each gradient, the column was again equilibrated to 5% B for 2 min. The flow rate was set to 300 nl/min. MS1 full scans were acquired with a resolution of 120,000, an injection time of 50 ms, and an automatic gain control target of 1×10^6. Dynamic exclusion was set to 30 s and only charge states between 3 and 8 were considered for fragmentation. MS2 spectra were acquired of the 20 most abundant precursor ions; the resolution was set to 30,000; the injection time was set to 128 ms, and the automatic gain control target to 1×10^5. Fragmentation was enforced by higher-energy collisional dissociation at 30% normalised collision energy.

Raw files were analyzed by pLink 2 (v. 2.3.9) (47) for the identification of crosslinked peptides with the following parameters: BS3 was selected as crosslinker, global false discovery rate was set to 5% on spectrum level, and the protein database contained the amino acid sequences of RelA and DarB.

Rel^{NTD}–DarB docking experiments

In silico docking experiments have been performed with Rel^{NTD} (PDB ID: 6YXA) and homodimeric DarB structure using a combination of the blind docking search (ClusPro (48) and HADDOCK (49) web servers) followed by high-resolution docking with the RosettaDock application (50). The former stage facilitates quick sampling of the available search space in an attempt to find the rough orientation of the docking partners for the later high-resolution docking. The high-resolution stage performs model optimization by rigid body adjustments alternated with side-chain repacking of the docked partners. For each of 299 ClusPro and 267 HADDOCK decoys at least 100 atomic models of Rel^{NTD}–DarB complexes have been generated using a high-resolution docking approach as implemented in RosettaDock. The high-resolution decoys have been scored based on their interface score (I_sc), representing the energy of the interactions across the interface, and clustered. Three Rel^{NTD}–DarB decoys, selected based on their I_sc score and originating from initial orientation predicted by ClusPro server, have been used to propose single point mutations of DarB, which should prevent complex formation. Mutagenesis of two out of three proposed residues of DarB (Asn68 and Leu38) have proven to disrupt complex formation with Rel^{NTD}. The corresponding Rel^{NTD}–DarB complex "low resolution" models revealed a difference in the position of DarB (up to ∼7 Å due to a rotational movement around DarB dimerization axis). Hence, the orientation of DarB has been manually adjusted using spatial distance constraints derived from crosslinking experiments followed by crosslinking guided docking as implemented in RosettaDock. Due to the fact that a vast number of crosslink derived spatial constraints were not compatible with the best "low resolution" Rel^{NTD}–DarB complex models, several sets of constraints have been generated based on the increased crosslink peptide-spectra matching (CSM) score. The main aim of the applied filtering of MS results was to obtain a set

of reliable constraints, which could be applied for both model validation and high-resolution docking. The CSM scores were used as thresholds for generating five sets of constraints (CSM ≥ 3, 4, 5, 6, 7), which have been visually inspected in PyMOL in the form of interatomic distances between NZ atoms (these atoms have been chosen to approximate in the best way the distance on the protein surface). The first set (CSM ≥ 3) comprised 22 spatial constraints while the last one (CSM ≥ 7) yielded nine constraints. The chosen approach resulted in obtaining a set of crosslink-based constraints (CSM scores ≥ 7) supporting the model. It has been utilized by RosettaDock protocol in a form of a flat harmonic function. This guarantees that the model will be penalized only if the Euclidean distance between the crosslinked residues exceeds the specified distance (for NZ-NZ 12–15 Å and CB-CB 23–25 Å). For lysine residues residing on a potentially flexible protein region, for example a loop, a larger tolerance value has been applied. The table with constraints has been added to Fig. S8.

The most energetically favored decoy (out of 5000) that fulfilled crosslink-derived constraints (CSM ≥ 7) has been chosen as the final model of Rel^{NTD}–DarB complex.

Data availability

Atomic coordinates and structure factors of the crystal structures presented in this article were deposited in the Protein Data Bank (PDB) with following codes: 6YJ7 (DarB-AMP), 6YJ8 (DarB-apo), 6YJ9 (DarB-cGAMP), 6YJA (DarB-cdiAMP).

The mass spectrometry proteomics data have been deposited to the ProteomeXchange Consortium *via* the PRIDE partner repository with the dataset identifier PXD033346. A Microsoft Excel file containing pivot table and processed MS data can be downloaded from supplementary data.

Supporting information—This article contains supporting information.

Acknowledgments—We are grateful to the staff of the EMBL-Outstation Hamburg (DESY PETRA-III beamlines P13 and P14, Germany) for the allocation of beam time and support during X-ray diffraction data collection.

Author contributions—R. F. conceptualization; P. N. validation; J. L. H., P. N., L. K., D. W., L. V., and A. L. investigation; J. L. H. and P. N. data curation; J. L. H. and P. N. writing–original draft; L. K., A. D., J. S., H. U., and R. F. writing–review & editing; A. D. supervision; J. S., H. U., and R. F. funding acquisition.

Funding and additional information—This work was supported by grants of the Deutsche Forschungsgemeinschaft (DFG), Germany within the Priority Program SPP1879 (to R. F. and J. S.) and INST186/1117 (to R. F.) as well as SFB860 to (H. U. and R. F.).

Conflict of interest—The authors declare that they have no conflicts of interest with the contents of this article.

Abbreviations—The abbreviations used are: CBS, cystathionine β-synthase; c-di-AMP, cyclic dimeric AMP; CSM, crosslink peptide-spectra matching; ITC, isothermal calorimetry; MS, mass spectrometry; PDB, Protein Data Bank.

References

1. Bateman, A. (1997) The structure of a domain common to archaebacteria and the homocystinuria disease protein. *Trends Biochem. Sci.* **22**, 12–13
2. Baykov, A. A., Tuominen, H. K., and Lahti, R. (2011) The CBS domain: A protein module with an emerging prominent role in regulation. *ACS Chem. Biol.* **6**, 1156–1163
3. Ereno-Orbea, J., Oyenarte, I., and Martinez-Cruz, L. A. (2013) CBS domains: ligand binding sites and conformational variability. *Arch. Biochem. Biophys.* **540**, 70–81
4. Anashkin, V. A., Baykov, A. A., and Lahti, R. (2017) Enzymes regulated *via* cystathionine beta-synthase domains. *Biochemistry (Mosc)* **82**, 1079–1087
5. Huynh, T. N., Choi, P. H., Sureka, K., Ledvina, H. E., Campillo, J., Tong, L., *et al.* (2016) Cyclic di-AMP targets the cystathionine beta-synthase domain of the osmolyte transporter OpuC. *Mol. Microbiol.* **102**, 233–243
6. Schuster, C. F., Bellows, L. E., Tosi, T., Campeotto, I., Corrigan, R. M., Freemont, P., *et al.* (2016) The second messenger c-di-AMP inhibits the osmolyte uptake system OpuC in Staphylococcus aureus. *Sci. Signal.* **9**, ra81
7. Corrigan, R. M., and Gründling, A. (2013) Cyclic di-AMP: another second messenger enters the fray. *Nat. Rev. Microbiol.* **11**, 513–524
8. Commichau, F. M., Dickmanns, A., Gundlach, J., Ficner, R., and Stülke, J. (2015) A jack of all trades: the multiple roles of the unique essential second messenger cyclic di-AMP. *Mol. Microbiol.* **97**, 189–204
9. He, J., Yin, W., Galperin, M. Y., and Chou, S. H. (2020) Cyclic di-AMP, a second messenger of primary importance: tertiary structures and binding mechanisms. *Nucl. Acids Res.* **48**, 2807–2829
10. Stülke, J., and Krüger, L. (2020) Cyclic di-AMP signaling in bacteria. *Annu. Rev. Microbiol.* **74**, 159–179
11. Commichau, F. M., Gibhardt, J., Halbedel, S., Gundlach, J., and Stülke, J. (2018) A delicate connection: c-di-AMP affects cell integrity by controlling osmolyte transport. *Trends Microbiol.* **26**, 175–185
12. Corrigan, R. M., Campeotto, I., Jeganathan, T., Roelofs, K. G., Lee, V. T., and Gründling, A. (2013) Systematic identification of conserved bacterial c-di-AMP receptor proteins. *Proc. Natl. Acad. Sci. U. S. A.* **110**, 9084–9089
13. Bai, Y., Yang, J., Zarrella, T. M., Zhang, Y., Metzger, D. W., and Bai, G. (2014) Cyclic di-AMP impairs potassium uptake mediated by a cyclic di-AMP binding protein in Streptococcus pneumoniae. *J. Bacteriol.* **196**, 614–623
14. Kim, H., Youn, S. J., Kim, S. O., Ko, J., Lee, J. O., and Choi, B. S. (2015) Structural studies of potassium transport protein KtrA regulator of conductance of K+ (RCK) C domain in complex with cyclic diadenosine monophosphate (c-di-AMP). *J. Biol. Chem.* **290**, 16393–16402
15. Gundlach, J., Dickmanns, A., Schröder-Tittmann, K., Neumann, P., Kaesler, J., Kampf, J., *et al.* (2015) Identification, characterization, and structure analysis of the cyclic di-AMP-binding PII-like signal transduction protein DarA. *J. Biol. Chem.* **290**, 3069–3080
16. Quintana, I. M., Gibhardt, J., Turdiev, A., Hammer, E., Commichau, F. M., Lee, V. T., *et al.* (2019) The KupA and KupB proteins of lactococcus lactis IL1403 are novel c-di-AMP receptor proteins responsible for potassium uptake. *J. Bacteriol.* **201**, e00028-19
17. Gundlach, J., Herzberg, C., Kaever, V., Gunka, K., Hoffmann, T., Weiss, M., *et al.* (2017) Control of potassium homeostasis is an essential function of the second messenger cyclic di-AMP in Bacillus subtilis. *Sci. Signal.* **10**, eaal3011
18. Gundlach, J., Krüger, L., Herzberg, C., Turdiev, A., Poehlein, A., Tascon, I., *et al.* (2019) Sustained sensing in potassium homeostasis: cyclic di-AMP controls potassium uptake by KimA at the levels of expression and activity. *J. Biol. Chem.* **294**, 9605–9614
19. Moscoso, J. A., Schramke, H., Zhang, Y., Tosi, T., Dehbi, A., Jung, K., *et al.* (2016) Binding of cyclic di-AMP to the Staphylococcus aureus sensor kinase KdpD occurs *via* the universal stress protein domain and

downregulates the expression of the kdp potassium transporter. *J. Bacteriol.* **198**, 98–110
20. Sureka, K., Choi, P. H., Precit, M., Delince, M., Pensinger, D. A., Huynh, T. N., *et al.* (2014) The cyclic dinucleotide c-di-AMP is an allosteric regulator of metabolic enzyme function. *Cell* **158**, 1389–1401
21. Rosenberg, J., Dickmanns, A., Neumann, P., Gunka, K., Arens, J., Kaever, V., *et al.* (2015) Structural and biochemical analysis of the essential diadenylate cyclase CdaA from Listeria monocytogenes. *J. Biol. Chem.* **290**, 6596–6606
22. Corrigan, R. M., Abbott, J. C., Burhenne, H., Kaever, V., and Grundling, A. (2011) c-di-AMP is a new second messenger in Staphylococcus aureus with a role in controlling cell size and envelope stress. *PLoS Pathog.* **7**, e1002217
23. Woodward, J. J., Iavarone, A. T., and Portnoy, D. A. (2010) c-di-AMP secreted by intracellular Listeria monocytogenes activates a host type I interferon response. *Science* **328**, 1703–1705
24. Jackson-Litteken, C. D., Ratliff, C. T., Kneubehl, A. R., Siletti, C., Pack, L., Lan, R., *et al.* (2021) The diadenylate cyclase CdaA is critical for Borrelia turicatae virulence and physiology. *Infect. Immun.* **89**, e00787-20
25. Peterson, B. N., Young, M. K. M., Luo, S., Wang, J., Whiteley, A. T., Woodward, J. J., *et al.* (2020) ppGpp and c-di-AMP homeostasis is controlled by CbpB in Listeria monocytogenes. *mBio* **11**, e01625-20
26. Krüger, L., Herzberg, C., Wicke, D., Bahre, H., Heidemann, J. L., Dickmanns, A., *et al.* (2021) A meet-up of two second messengers: the c-di-AMP receptor DarB controls (p)ppGpp synthesis in Bacillus subtilis. *Nat. Commun.* **12**, 1210
27. Cashel, M., and Gallant, J. (1969) Two compounds implicated in the function of the RC gene of Escherichia coli. *Nature* **221**, 838–841
28. Dalebroux, Z. D., and Swanson, M. S. (2012) ppGpp: magic beyond RNA polymerase. *Nat. Rev. Microbiol.* **10**, 203–212
29. Krüger, L., Herzberg, C., Wicke, D., Scholz, P., Schmitt, K., Turdiev, A., *et al.* (2022) Sustained control of pyruvate carboxylase by the essential second messenger cyclic di-AMP in Bacillus subtilis. *Mbio* **13**, e0360221
30. Chin, K.-H., Liang, J.-M., Yang, J.-G., Shih, M.-S., Tu, Z.-L., Wang, Y.-C., *et al.* (2015) Structural insights into the distinct binding mode of cyclic di-AMP with SaCpaA_RCK. *Biochemistry* **54**, 4936–4951
31. Pausch, P., Abdelshahid, M., Steinchen, W., Schafer, H., Gratani, F. L., Freibert, S. A., *et al.* (2020) Structural basis for regulation of the opposing (p)ppGpp synthetase and hydrolase within the stringent response orchestrator Rel. *Cell Rep.* **32**, 108157
32. Choi, P. H., Vu, T. M. N., Pham, H. T., Woodward, J. J., Turner, M. S., and Tong, L. (2017) Structural and functional studies of pyruvate carboxylase regulation by cyclic di-AMP in lactic acid bacteria. *Proc. Natl. Acad. Sci. U. S. A.* **114**, E7226–E7235
33. McLean, J. E., Hamaguchi, N., Belenky, P., Mortimer, S. E., Stanton, M., and Hedstrom, L. (2004) Inosine 5'-monophosphate dehydrogenase binds nucleic acids *in vitro* and *in vivo*. *Biochem. J.* **379**, 243–251
34. Aguado-Llera, D., Oyenarte, I., Martinez-Cruz, L. A., and Neira, J. L. (2010) The CBS domain protein MJ0729 of Methanocaldococcus jannaschii binds DNA. *FEBS Lett.* **584**, 4485–4489
35. Sambrook, J., Fritsch, E. F., and Maniatis, T. (1989) *Molecular Cloning: A Laboratory Manual*, 2nd ed., Cold Spring Harbor Laboratory, Cold Spring Harbor, NY
36. Kunst, F., and Rapoport, G. (1995) Salt stress is an environmental signal affecting degradative enzyme synthesis in Bacillus subtilis. *J. Bacteriol.* **177**, 2403–2407
37. Bi, W., and Stambrook, P. J. (1998) Site-directed mutagenesis by combined chain reaction. *Anal. Biochem.* **256**, 137–140
38. Bradford, M. M. (1976) A rapid and sensitive method for the quantitation of microgram quantities of protein utilizing the principle of protein-dye binding. *Anal. Biochem.* **72**, 248–254
39. Kabsch, W. (2010) XDS. *Acta Crystallogr. D Biol. Crystallogr.* **66**, 125–132
40. Kabsch, W. (2010) Integration, scaling, space-group assignment and post-refinement. *Acta Crystallogr. D Biol. Crystallogr.* **66**, 133–144
41. McCoy, A. J., Grosse-Kunstleve, R. W., Adams, P. D., Winn, M. D., Storoni, L. C., and Read, R. J. (2007) Phaser crystallographic software. *J. Appl. Crystallogr.* **40**, 658–674
42. Emsley, P., Lohkamp, B., Scott, W. G., and Cowtan, K. (2010) Features and development of Coot. *Acta Crystallogr. D Biol. Crystallogr.* **66**, 486–501
43. Winn, M. D., Ballard, C. C., Cowtan, K. D., Dodson, E. J., Emsley, P., Evans, P. R., *et al.* (2011) Overview of the CCP4 suite and current developments. *Acta Crystallogr. D Biol. Crystallogr.* **67**, 235–242
44. Adams, P. D., Afonine, P. V., Bunkoczi, G., Chen, V. B., Davis, I. W., Echols, N., *et al.* (2010) PHENIX: a comprehensive python-based system for macromolecular structure solution. *Acta Crystallogr. D Biol. Crystallogr.* **66**, 213–221
45. Liebschner, D., Afonine, P. V., Moriarty, N. W., Poon, B. K., Sobolev, O. V., Terwilliger, T. C., *et al.* (2017) Polder maps: improving OMIT maps by excluding bulk solvent. *Acta Crystallogr. D Struct. Biol.* **73**, 148–157
46. Leitner, A., Reischl, R., Walzthoeni, T., Herzog, F., Bohn, S., Forster, F., *et al.* (2012) Expanding the chemical cross-linking toolbox by the use of multiple proteases and enrichment by size exclusion chromatography. *Mol. Cell Proteomics* **11**, M111.014126
47. Chen, Z. L., Meng, J. M., Cao, Y., Yin, J. L., Fang, R. Q., Fan, S. B., *et al.* (2019) A high-speed search engine pLink 2 with systematic evaluation for proteome-scale identification of cross-linked peptides. *Nat. Commun.* **10**, 3404
48. Kozakov, D., Hall, D. R., Xia, B., Porter, K. A., Padhorny, D., Yueh, C., *et al.* (2017) The ClusPro web server for protein-protein docking. *Nat. Protoc.* **12**, 255–278
49. van Zundert, G. C. P., Rodrigues, J., Trellet, M., Schmitz, C., Kastritis, P. L., Karaca, E., *et al.* (2016) The HADDOCK2.2 web server: user-friendly integrative modeling of biomolecular complexes. *J. Mol. Biol.* **428**, 720–725
50. Chaudhury, S., Berrondo, M., Weitzner, B. D., Muthu, P., Bergman, H., and Gray, J. J. (2011) Benchmarking and analysis of protein docking performance in Rosetta v3.2. *PLoS One* **6**, e22477